Supporting Information for

Covalently grafting covalent organic framework onto carbon nanotubes as bifunctional electrocatalyst for overall water splitting

Hongwei Li,[a] Qizhe He[a], Yunye Cao,*[a] Lei Lei,[b] Degao Wang,*[bc] Ting-Ting Li*[a]

[a]School of Materials Science and Chemical Engineering, Ningbo University, Ningbo, Zhejiang, 315211, China. E-mail: litingting@nbu.edu.cn; caoyunye@nbu.edu.cn.

[b]Engineering Laboratory of Advanced Energy Materials, Ningbo Institute of Materials Technology and Engineering, Chinese Academy of Sciences, Ningbo, Zhejiang, 315201, China. wangdegao@nimte.ac.cn.

[c]Research Center for Advanced Interdisciplinary Sciences, Ningbo Institute of Materials Technology and Engineering, Chinese Academy of Sciences, Ningbo, Zhejiang, 315201, China.

Materials and Methods

Materials

All chemicals were purchased from commercial sources and used without further treatment. Potassium hydroxide, dioxane, mesitylene, $Ni(OAc)_2 \cdot 4H_2O$, acetic acid (HOAc), tetrahydrofuran (THF), and isopropyl alcohol were purchased from Aladdin Biochemical Technology Co., Ltd. Nafion solution (5 wt %) was purchased from Alfa Aesar Co., Ltd. Carbon nanotubes (CNTs) were purchased from Jiangsu XFNANO Materials Tech Co., Ltd. Amino-functionalized carbon nanotubes (NCNTs), methanol (99.9%) were purchased from PETSUN Co., Ltd. 2,2′-bipyridine-5,5′-diamine (Bpy) and 1,3,5-triformylphloroglucinol (Tp) were purchased from Leyan Co., Ltd.

Synthesis of TpBpy, NiTpBpy, NiTpBpy@CNTs, NiTpBpy@NCNTs

The synthesis of TpBpy in this study follows a previously reported method but with a slight modification.[1] Initially, in a 10 mL Pyrex tube, Tp (21.0 mg, 0.1 mmol), Bpy (27.9 mg, 0.15 mmol), mesitylene (1.5 mL), dioxane (1.5 mL), and 6 M HOAc (0.3 mL) were added. The mixture was then sonicated for 30 minutes and degassed through three freeze-pump-thaw cycles before being sealed under vacuum. The sealed tube was subsequently placed in an oven at 120 ℃ for 3 days and then cooled to room temperature. The resulting precipitate was collected by filtration, and washed with THF and acetone multiple times. The product was then Soxhlet extracted with THF and acetone for 2 days and dried under vacuum at 60 ℃ for 24 hours, affording TpBpy (39.1 mg, yield: 80.1 %). To incorporate

Ni(II) ions into the COF, 50 mg of the synthesized TpBpy was treated with $Ni(OAc)_2 \cdot 4H_2O$ (20 mg) dissolved in 20 mL of dry methanol. The resulting solution was stirred for 6 hours at room temperature and then washed with a copious amount of dry methanol. The obtained NiTpBpy was activated using a vacuum overnight at 60 ℃.

NiTpBpy@CNTs and NiTpBpy@NCNTs were synthesized using the same process with the addition of CNTs (122.2 mg) or NCNTs (122.2 mg) as the scaffold at the synthesis step.

Physical Characterizations

Powder X-ray diffraction (PXRD) patterns of the samples were recorded using an X-ray diffractometer (Bruker D8 Advance) with a Cu Kα radiation source at 1600 W (40 kV voltage, 40 mA) power. Fourier transform infrared (FT-IR) spectroscopy was performed using an FT-IR spectrometer (Thermo Scientific Nicolet iS20) in a wavenumber range of 4000 ~ 400 cm^{-1}. The metal content of the sample was determined by inductively coupled plasma optical emission spectroscopy (ICP-OES, Thermo Fisher iCAPPRO). Scanning electron microscopy (SEM) was carried out using a FEI Nova NanoSEM 450 scanning electron microscope with an accelerating voltage of 5 kV. Transmission electron microscopy (TEM) and high-resolution TEM (HR-TEM) were performed using a FEI Tecnai G2 F20 electron microscope equipped with an elemental mapping and energy dispersive spectroscopy (EDS) detector and operated at an accelerating voltage of 200 kV. The surface chemical composition of the samples was determined by in-situ electrochemical confocal Raman micro-spectroscopy using a Raman spectrometer (UniDRON) equipped with a 532 nm laser source and an Olympus × 50 Lwd objective. The scanning range was from 200 to 800 cm^{-1}. The resolution of the Raman spectrum was 4 cm^{-1}. The electrochemical cell, designed and constructed in-house, was based on a round Teflon-lined dish. To meet the experimental requirements, the electrochemical cell was filled with a 1 M KOH solution. Different voltages were applied from 1.0 to 2.2 V vs RHE, and each voltage was tested for 1200 s. The Brunauer-Emmett-Teller (BET) specific surface area was measured on an apparatus (ASAP 2020) via adsorption-desorption isotherm at 77 K. X-ray photoelectron spectroscopy (XPS) measurement was recorded on a Thermo Scientific K-Alpha XPS system using C 1s (284.8 eV) as the reference binding energy. X-ray absorption fine structure spectra (Ni K-edge) were recorded at a laboratory device (easyXAFS300+, easyXAFS LLC), which is based on Rowland circle geometries with spherically bent crystal analyzers (SBCA) and operated by a Mo X-ray tube source and a silicon drift detector (AXAS-M2, KETEK GmbH) using a silicon double-crystal monochromator.[2] Before X-ray absorption fine structure (XAFS) measurement, the sample was uniformly grounded and then pressed into a wafer with a thickness of ~1 mm by a tablet press. The wafer was fixed with the special adhesive tape on the 8-position automatic sample wheel. The data collection was

finished in transmission mode for the samples of Ni foil, NiPc, NiO, and NiTpBpy. All pristine spectra data were collected in ambient conditions. The obtained XAFS data was processed in Athena software (version 0.9.26) for background, pre-edge line, and post-edge line calibrations. Then Fourier transformed fitting was carried out in Artemis software (version 0.9.26). For EXAFS modeling, EXAFS of the Ni foil is fitted, and the obtained amplitude reduction factor S_0^2 =0.75 was set in the EXAFS analysis to determine the coordination numbers in NiTpBpy. For Wavelet Transform analysis, the χ(k) exported from Athena was imported into the Matlab. The parameters were listed as follows: R range, 0 ~ 6 Å, k range, 0 ~ 12 $Å^{-1}$ for Ni foil, NiO, NiPc, and NiTpBpy; k weight, 3; Morlet function with κ = 5, σ = 1 was used as the mother wavelet to provide the overall distribution.

Electrode preparation

The 1 cm × 1.5 cm pieces of carbon cloth were first subjected to a 30-minute sonication process in ethanol and acetone solutions to eliminate surface carbon deposits and oil contamination. To enhance the hydrophilicity of carbon cloth, a sequential process is carried out. Initially, the carbon cloth was immersed in a round-bottomed flask containing concentrated sulfuric acid and concentrated nitric acid, with a volume ratio of 3:1, followed by heating at 70 ℃ for 8 hours. Subsequently, it was rinsed several times with deionized water to eliminate any remaining acids. To ensure the complete elimination of sulfuric acid and nitric acid residues, the carbon cloth was sonicated in deionized water until the pH of the solution reached approximately 7. Afterward, the carbon cloth was dried overnight at 100 ℃ in an oven. To prepare the catalyst ink, the catalyst was dispersed in a mixed solution of isopropanol, water, and 5 wt % Nafion was added to formulate a catalyst ink of 1.0 mg mL^{-1}. Then, 200 μL of the ink was deposited uniformly onto the carbon cloth (1 × 1 cm^2) to achieve a working electrode with a catalyst loading amount of 0.2 mg cm^{-2}. Finally, the electrode was dried overnight at room temperature.

Preparation of Pt/C and RuO_2 electrodes

Typically, 2.5 mg of commercial RuO_2 or Pt/C (20 wt%) was dispersed in a mixture solution with DI water (400 μL), absolute ethanol (560 μL), and Nafion solution (5 wt%, 40 μL), and then ultra-sonicated to form a homogeneous catalyst ink. RuO_2 or Pt/C electrode was obtained by uniformly dropping 80 μL of the catalyst ink onto the treated carbon cloth (1 × 1 cm^2) and finally drying overnight at room temperature.

Electrochemical measurements

The electrochemical measurements were carried out on an electrochemical workstation (CHI 760E) with a three-electrode system at room temperature. In the standard three-electrode system, Ag/AgCl and graphite rod or Platinum mesh served as the reference electrode and the counter electrode, respectively. The overall water splitting experiment

was performed by a two-electrode system of carbon cloth (1 × 1 cm^{-2}) with catalyst loading of 0.2 mg cm^{-2} after a similar process. Electrochemical measurements were performed in 1 M KOH solution, while N_2 and O_2 were introduced into the KOH solution to saturation before the HER and OER testing, respectively. The reversible hydrogen electrode (RHE) was calibrated to all of the potentials referenced in this study, based on the equation: $E_{(RHE)} = E_{Ag/AgCl} + 0.197 + 0.059 \times pH$. The polarization curves of the HER or OER were examined by linear sweep voltammetry (LSV) measurement at a scan rate of 5 mV s^{-1} with 95% iR compensation for the OER and 80% iR compensation for the HER, and the value of the Tafel slope was calculated from the corresponding LSV plots. Cyclic voltammetry (CV) curves for the OER were recorded at different scan rates (20, 40, 60, 80, and 100 mV s^{-1}) in the potential range of 1.1 ~ 1.2 V vs RHE, and each Δj/2 was calculated at 1.15 V vs RHE to evaluate the double-layer capacitance (C_{dl}) values. CV curves for the HER were recorded at different scan rates (20, 40, 60, 80, and 100 mV s^{-1}) in the potential range of 0.1 ~ 0.2 V vs RHE, and each Δj/2 was calculated at 0.15 V vs RHE to evaluate the C_{dl} values. The chronoamperometry tests for HER and OER stability evaluation were conducted at −0.41 V vs RHE and 1.59 V vs RHE, respectively. Electrochemical impedance spectroscopy (EIS) analysis was examined at a certain overpotential of 150 mV for the HER in the frequency range from 10^{-2} to 10^5 Hz with a sinusoidal amplitude of 5 mV.

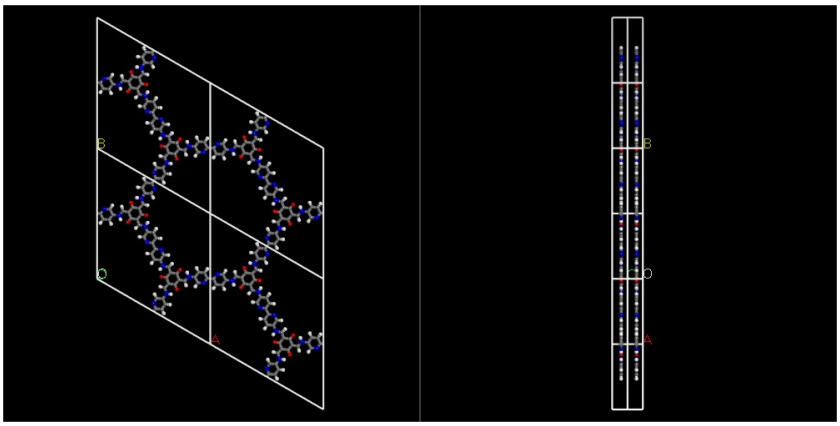

Fig. S1. Top and side views of the AA stacking structure of TpBpy (gray, C; blue, N; red, O; white, H).

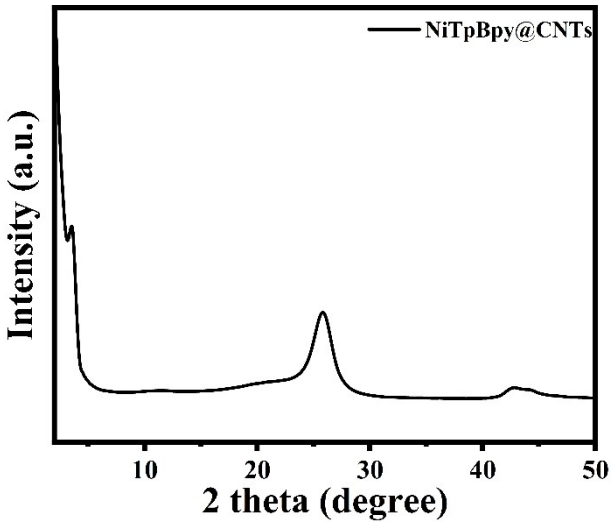

Fig. S2. PXRD patterns of NiTpBpy@CNTs.

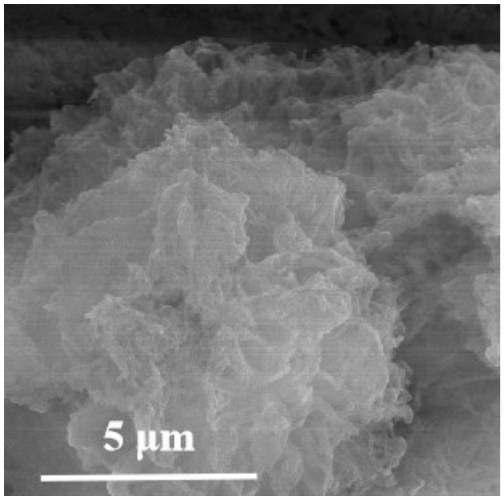

Fig. S3. SEM image of TpBpy.

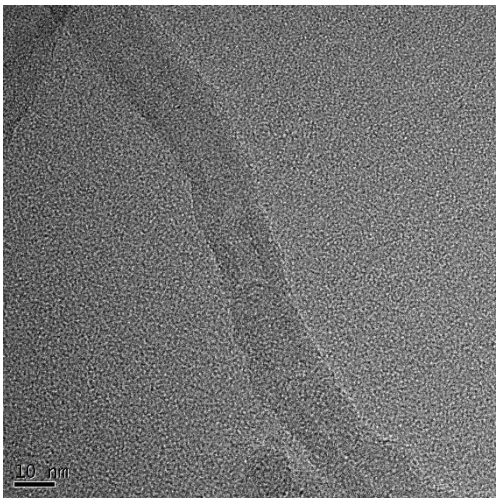

Fig. S4. TEM image of NCNTs.

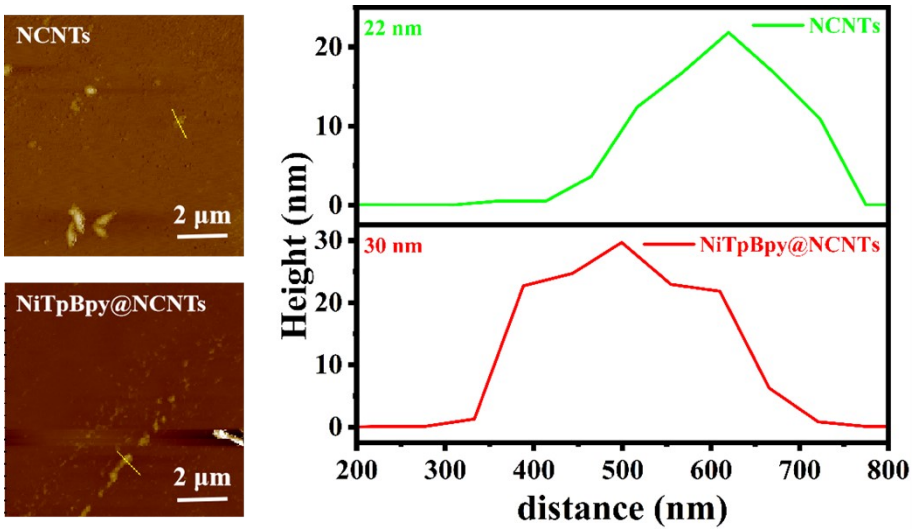

Fig. S5. AFM images of NCNTs and NiTpBpy@NCNTs.

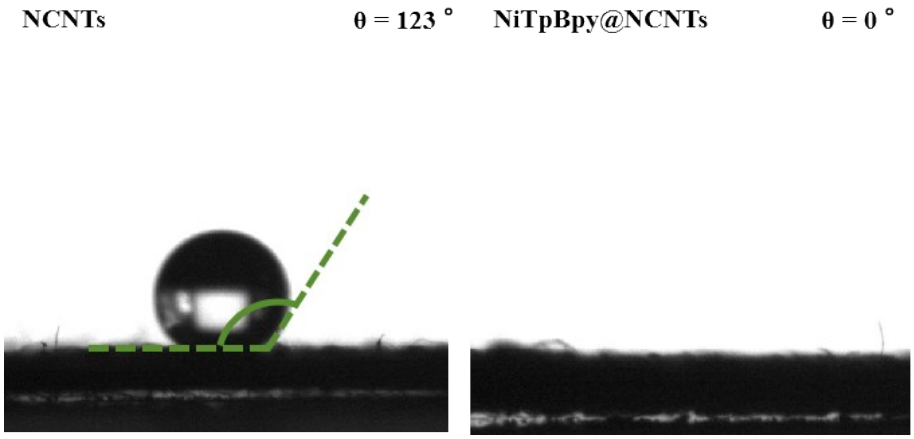

Fig. S6. The contact angles of NCNTs and NiTpBpy@NCNTs at the solid-liquid interface.

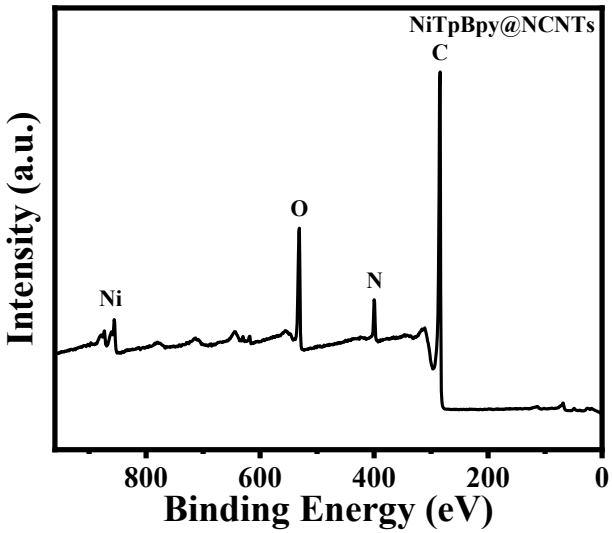

Fig. S7. The XPS survey spectrum of NiTpBpy@NCNTs.

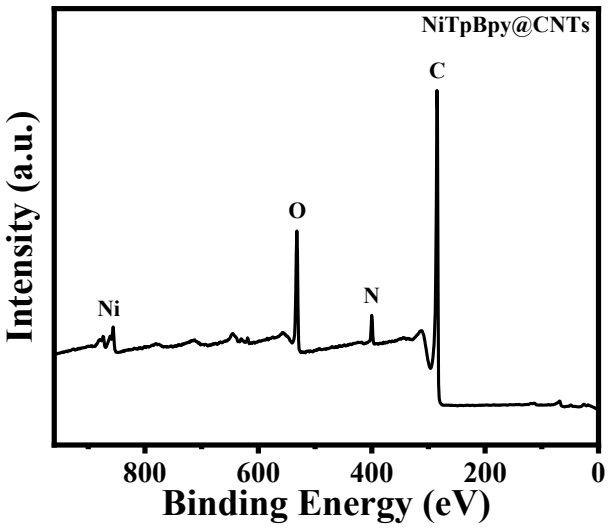

Fig. S8. The XPS survey spectrum of NiTpBpy@CNTs.

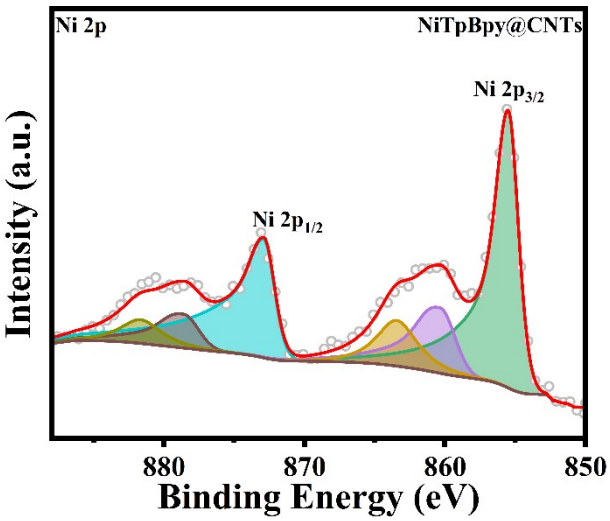

Fig. S9. High-resolution Ni 2p XPS spectrum of NiTpBpy@CNTs.

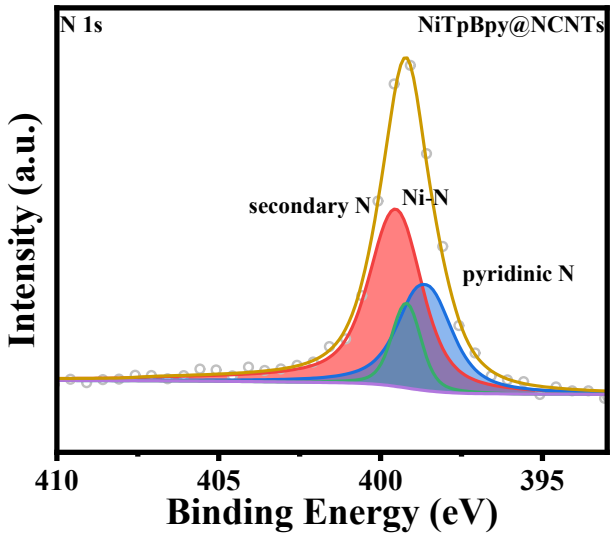

Fig. S10. High-resolution N 1s XPS spectrum of NiTpBpy@NCNTs.

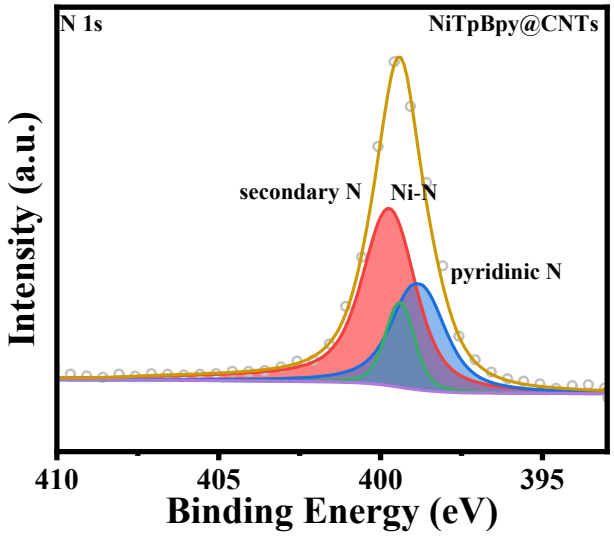

Fig. S11. High-resolution N 1s XPS spectrum of NiTpBpy@CNTs.

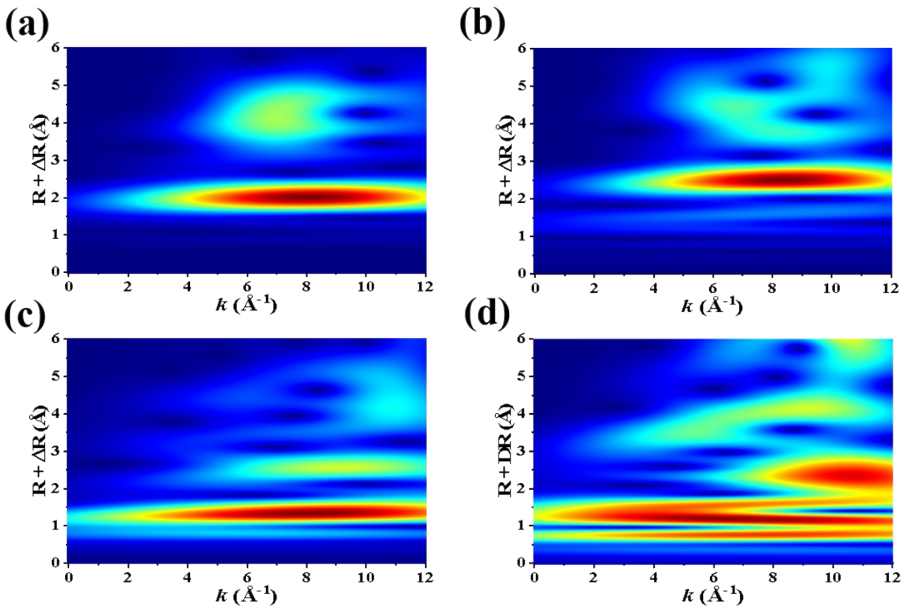

Fig. S12. The WT-EXAFS analysis of (a) Ni foil, (b) NiO, (c) NiPc, and (d) NiTpBpy.

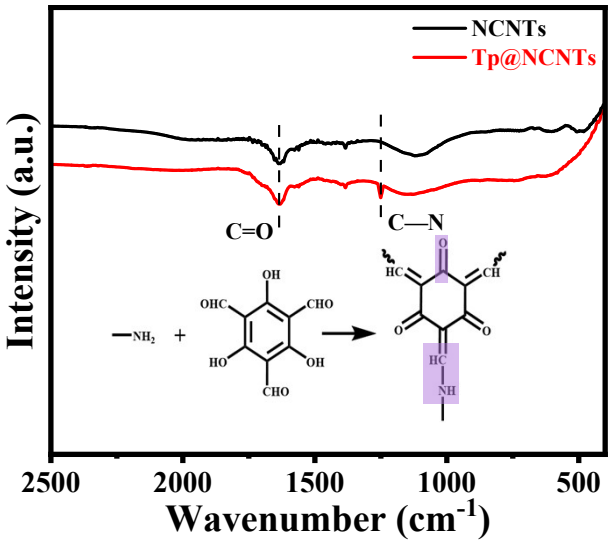

Fig. S13. FT-IR spectra of NCNTs and Tp@NCNTs.

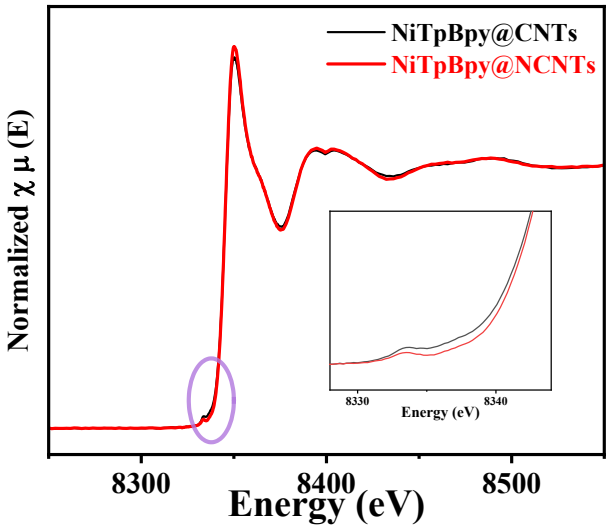

Fig. S14. Normalized Ni K-edge XANES spectra for NiTpBpy@CNTs and NiTpBpy@NCNTs.

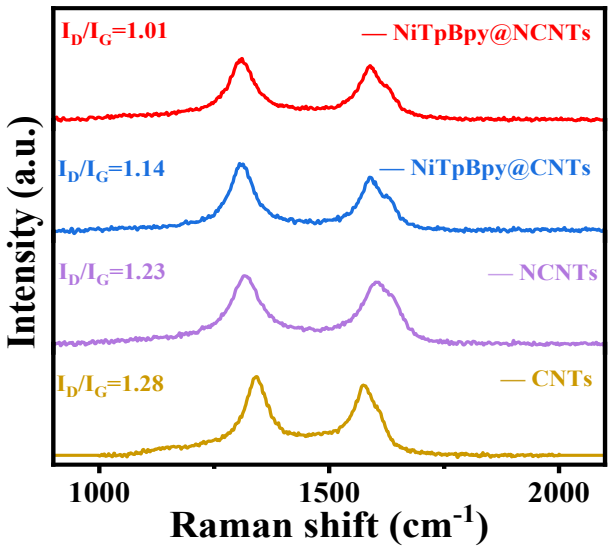

Fig. S15. Raman spectra of CNTs, NCNTs, NiTpBpy@CNTs, and NiTpBpy@NCNTs.

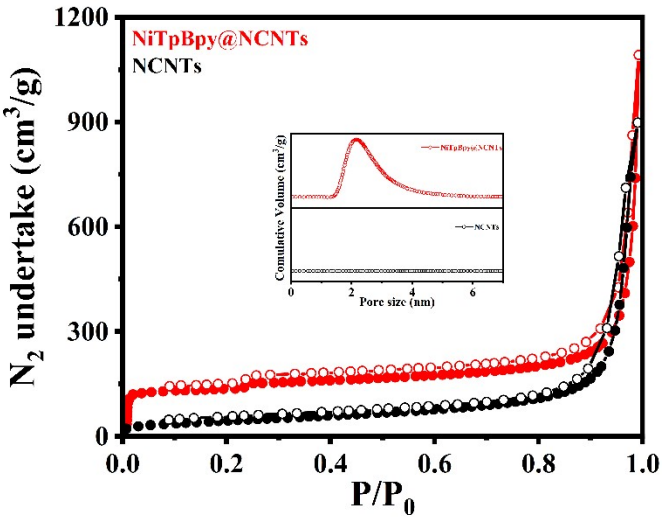

Fig. S16. Nitrogen adsorption-desorption isotherms of NiTpBpy@NCNTs and NCNTs. (Inset) The corresponding curves of pore size distribution.

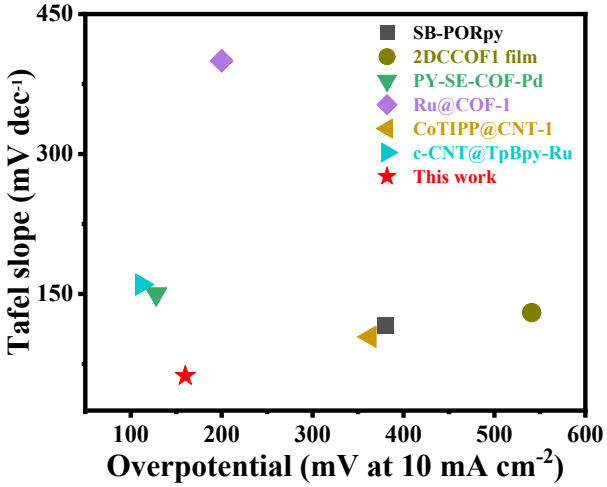

Fig. S17. Comparison of the HER activity of NiTpBpy@NCNTs with recently reported COFs-based HER electrocatalysts.

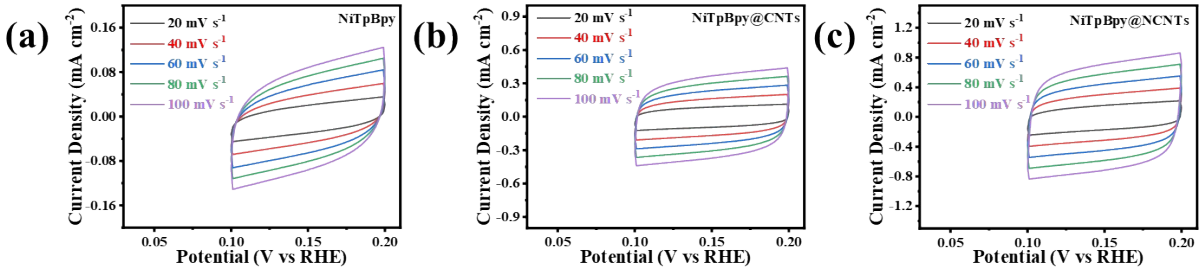

Fig. S18. CV plots for (a) NiTpBpy, (b) NiTpBpy@CNTs, and (c) NiTpBpy@NCNTs.

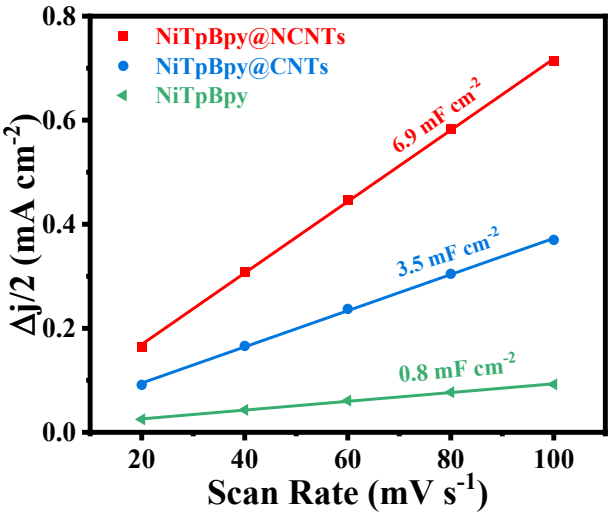

Fig. S19. Electrochemical double-layer capacitances for NiTpBpy@NCNTs, NiTpBpy@CNTs, and NiTpBpy.

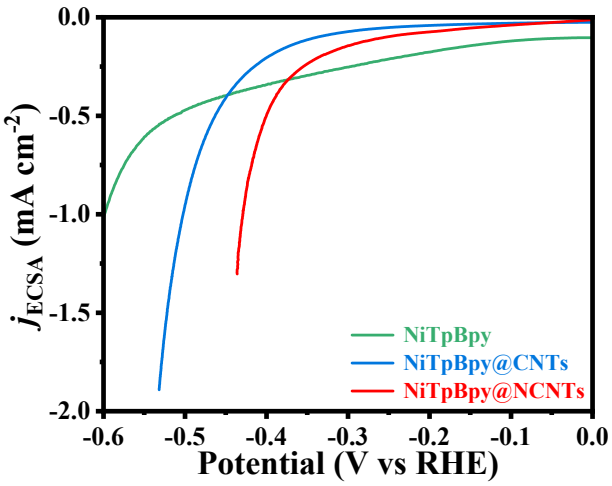

Fig. S20. ECSA-normalized LSV curves of NiTpBpy, NiTpBpy@CNTs, and NiTpBpy@NCNTs.

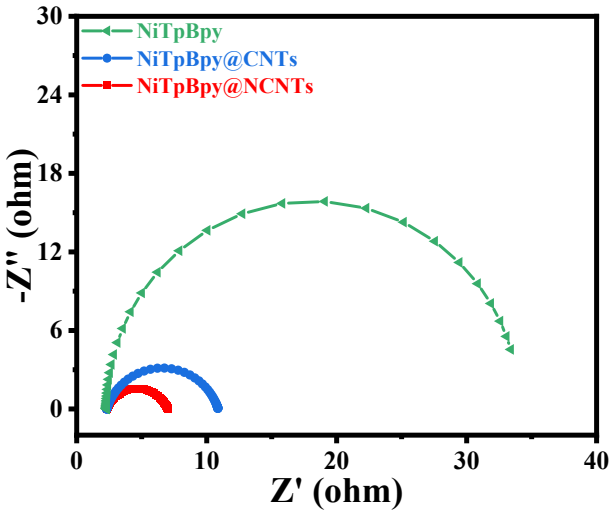

Fig. S21. Nyquist plots of NiTpBpy, NiTpBpy@CNTs, and NiTpBpy@NCNTs.

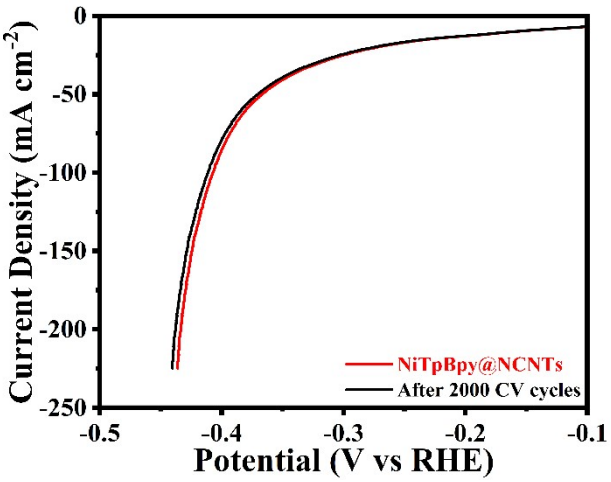

Fig. S22. The LSV curves of NiTpBpy@NCNTs before and after 2000 CV cycles.

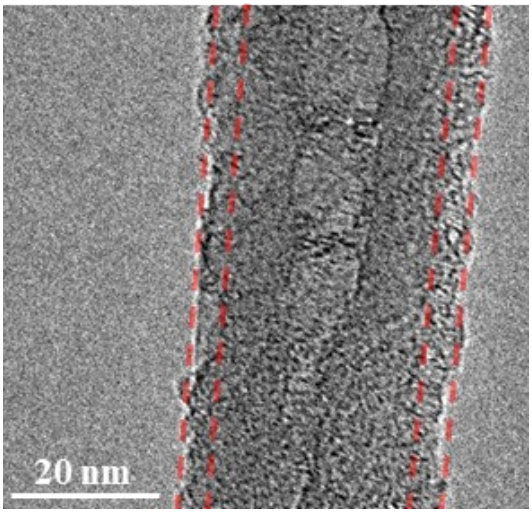

Fig. S23. TEM image of NiTpBpy@NCNTs after the HER stability test.

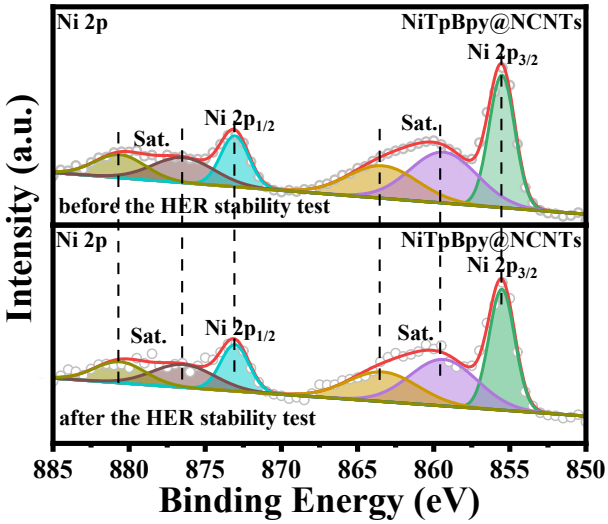

Fig. S24. Ni 2p XPS spectra of NiTpBpy@NCNTs before and after the HER stability test.

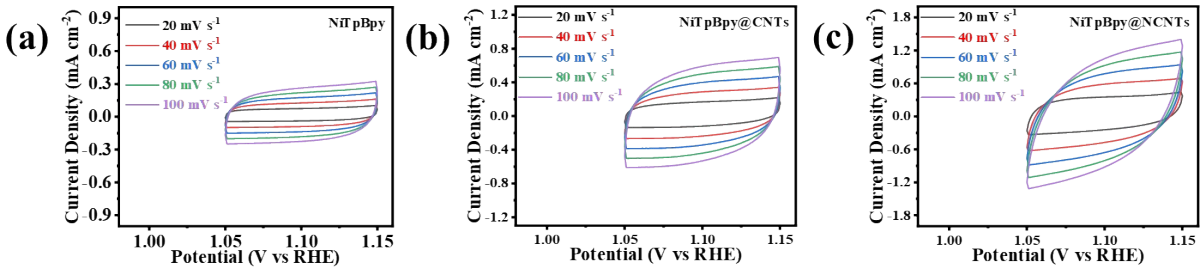

Fig. S25. CV plots for (a) NiTpBpy, (b) NiTpBpy@CNTs, and (c) NiTpBpy@NCNTs.

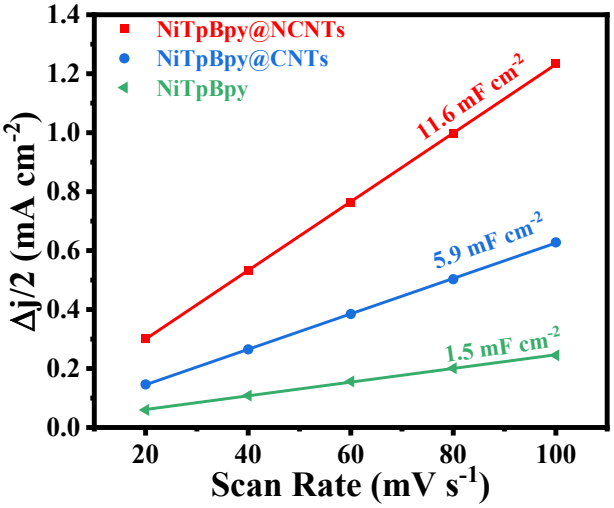

Fig. S26. Electrochemical double-layer capacitances for NiTpBpy@NCNTs, NiTpBpy@CNTs, and NiTpBpy.

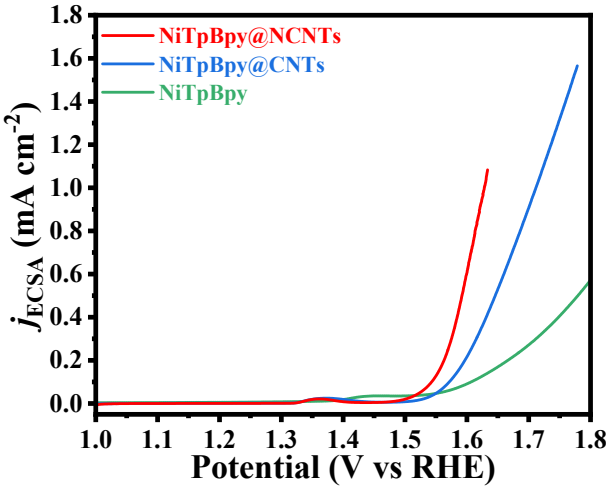

Fig. S27. The ECSA-normalized LSV curves of NiTpBpy, NiTpBpy@CNTs, and NiTpBpy@NCNTs.

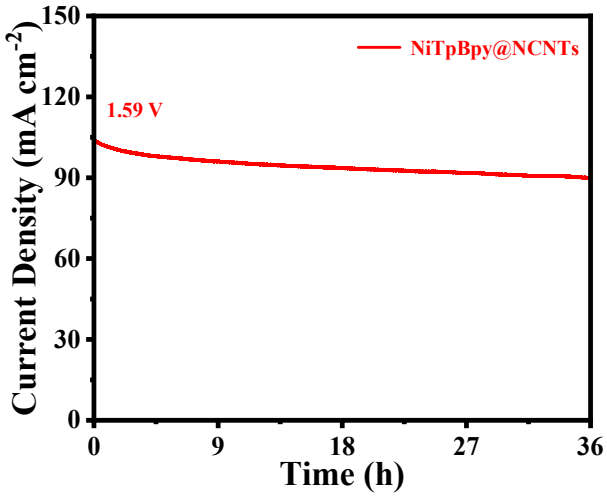

Fig. S28. Long-term stability test of NiTpBpy@NCNTs at 1.59 V vs RHE.

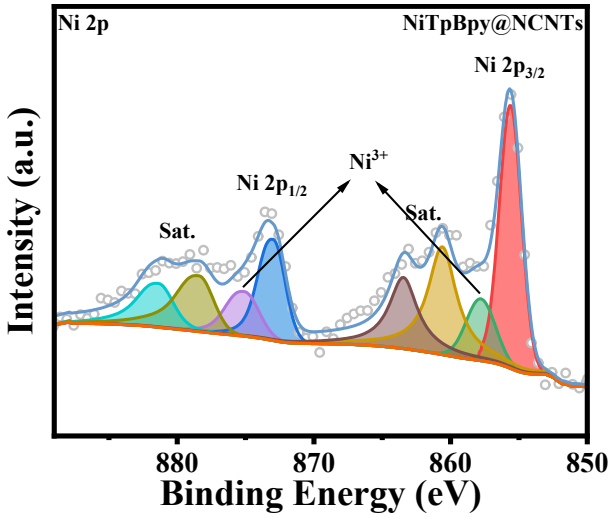

Fig. S29. Ni 2p XPS spectrum of NiTpBpy@NCNTs after the OER stability test.

Table S1. The Ni contents for the prepared samples determined by ICP-OES.

Sample	Ni(II) content (wt%)
NiTpBpy	10.52
NiTpBpy@NCNTs	3.11
NiTpBpy@CNTs	3.07

Table S2. The EXAFS fitting results include coordination number (CN), Debye-Waller factor (σ^2), inner potential correction (ΔE_0), and bond distance (R).

Sample	Paths	CN	σ^2	ΔE_0	R (Å)
NiTpBpy	Ni–O	2.006	0.00166	-3.185	1.99215
	Ni–N	2.006	0.00025		2.08988

Table S3. Summary of the previously reported COFs-based HER and OER electrocatalysts and their electrocatalytic performance.

COFs-based electrocatalysts	Electrocatalytic reaction	Mass loading of electrocatalyst (mg cm^{-2})	η_{10} (mV)	Tafel slope (mV dec^{-1})	Ref.
SB-PORpy	HER	–	η_5 = 380	116	3
PY-SE-COF	HER	–	–	263	4
2DCCOF1 film	HER	–	541	130	5
BPT-COF-rGO	HER	–	45	53	6
CoTcPP	HER	0.08	475	–	7
PY-SE-COF-Pd	HER	–	128	150	4
Ru@COF-1	HER	–	200	140	8
CoTIPP@CNT-1	HER	0.51	363	104	9
c-CNT@TpBpy-Ru	HER	0.5	112	160	10
NiTpBpy@NCNTs	HER	0.2	160	62.2	this work
IISERP-COF3	OER	0.005	400	–	11
Tp-Tta COF	OER	1	430	129	12
C4-SHz COF	OER	0.07	320	39	13
JUC-630	OER	–	400	104	14

Co-TpBpy	OER	–	η_1 = 400	59	15
Macro-TpBpy-Co	OER	0.25	380	54	16
CoTAPP-PATA-COF	OER	0.2	420	56	17
CoTAPP-BDTA-COF	OER	0.2	470	57	17
NiTAPP-PATA-COF	OER	0.2	670	–	17
FeTAPP-PATA-COF	OER	0.2	550	–	17
ZJTU-1@Co	OER	4	295	63	17
H_2NiPcCOF	OER	3	>430	68	18
NiPcCOF	OER	3	410	75	18
H_2FePcCOF	OER	3	430	62	18
H_2FeNiPcCOF	OER	3	430	78	18
$Ni_{0.5}Fe_{0.5}$@COF-SO_3	OER	–	300	83	19
COF-TpDb-TZ-Co	OER	–	390	82	20
Co_xNi_y-IISERP-COF2	OER	0.02	258	39	21
Ni_3N-IISERP-COF3	OER	0.07	230	79	22
Fe-SAC@COF	OER	1	290	40	12
Ni-SAC@COF	OER	1	337	45	12
Fe-NP/COF	OER	1	359	51	12
NiTIPP@CNT-2	OER	0.51	320	57	8
COF-366-Co@CNT	OER	–	358	62	23
NiTpBpy@NCNTs	OER	0.2	280	59.1	this work

Table S4. Summary of the previously reported COFs-based electrocatalysts for overall water splitting in an alkaline two-electrode system.

catalyst	electrolyte	cell voltage (V) at10 mA cm^{-2}	Ref.
CoTIPP@CNT-1	1.0 M KOH	2.04	9
CoTAPP-COF-Fe	1.0 M KOH	1.80	24
FeTPP@NiTPP/NF	1.0 M KOH	1.62	25
NiTpBpy@NCNTs	1.0 M KOH	1.59	this work

	1.83 @ 100 mA cm^{-2}

References

1 Q. Sun, B. Aguila, J. Perman, N. Nguyen and S. Ma, *J. Am. Chem. Soc.,* 2016, **138**, 15790-15796.

2 E. P. Jahrman, W. M. Holden, A.S. Ditter, D. R. Mortensen, G. T. Seidler, T. T. Fister, S. A. Kozimor, L. F. J. Piper, J. Rana, N. C. Hyatt and M. C. Stennett, *Sci. Instrum.*, 2019, **90**,024106.

3 S. Bhunia, S. K. Das, R. Jana, S. C. Peter, S. Bhattacharya, M. Addicoat, A. Bhaumik and A. Pradhan, *ACS Appl. Mater. Interfaces,* 2017, **9**, 23843.

4 J.Yue, X. Ding, L. Song, Y. Wang, P. Yang, Y. Ma and B. Tang, *Micropor. Mesopor. Mater.,* 2022, **344**, 112169.

5 D. Zhou, X. Tan, H. Wu, L. Tian and M. Li, *Angew. Chem. Int. Ed.,* 2019, **58**, 1376.

6 Y. Bai, Y. Liu, M. Liu, X. Wang, S. Shang, W. Gao, C. Du, Y. Qiao, J. Chen, J. Dong and Y. Liu, *Angew. Chem. Int. Ed.,* 2022, **61**, e202113067.

7 Y. Wu, J. M. Veleta, D. Tang, A. D. Price, C. E. Botez and D. Villagrán, *Dalt. Trans.,* 2018, **47**, 8801.

8 Y. Zhao, Y. Liang, D. Wu, H. Tian, T. Xia, W. Wang, W. Xie, X. Hu, W. Tian and Q. Chen, *Small,* 2022, **18**, 2107750.

9 Y. Wang, D. Song, J. Li, Q. Shi, J. Zhao, Y. Hu, F. Zeng and N. Wang, *Inorg. Chem.,* 2022, **61**, 10198-10204.

10 X. Sun, Y. Hu, Y. Fu, J. Yang, D. Song, B. Li, W. Xu and N. Wang, *Small,* 2024, **20**, 2305978.

11 S. Nandi, S. K. Singh, D. Mullangi, R. Illathvalappil, L. George, C. P. Vinod, S. Kurungot and R. Vaidhyanathan, *Adv. Energy Mater.,* 2016, **6**, 1601189.

12 Wang, X.; Sun, L.; Zhou, W.; Yang, L.; Ren, G.; Wu, H.; Deng, W. Q. Iron single-atom catalysts confined in covalent organic frameworks for efficient oxygen evolution reaction. *Cell Reports Phys. Sci.,* **2022**, *3*, 100804.

13 S. Mondal, B. Mohanty, M. Nurhuda, S. Dalapati, R. Jana, M. Addicoat, A. Datta, B. K. Jena and A. Bhaumik, *ACS Catal.,* 2020, **10**, 5623.

14 W. Xia, C. Ji, R. Wang, S. Qiu and Q. Fang, Q. *Acta Phys. Chim. Sin.,* 2023, **39**, 1-7.

15 H. B. Aiyappa, J. Thote, D. B. Shinde, R. Banerjee and S. Kurungot, *Chem. Mater.,* 2016, **28**, 4375.

16 X. Zhao, P. Pachfule, S. Li, T. Langenhahn, M. Ye, C. Schlesiger, S. Praetz, J. Schmidt and A. Thomas, *J. Am. Chem. Soc.,* 2019, **141**, 6623.

17 M. Liu, S. Liu, C. Cui, Q. Miao, Y. He, X. Li, Q. Xu and G. Zeng, *Angew. Chem. Int. Ed.,* 2022, **61**, e202213522.

18 J. J. Jarju, A. M. Díez, L. Frey, V. Sousa, E. Carbó-Argibay, L. P. L. Gonçalves, D. D. Medina, O. I. Lebedev, Y. V. Kolen'ko and L. M. Salonen, *Mater. Today Chem.,* 2022, 26, 101032.

19 Z. Gao, L. L. Gong, X. Q. He, X. Su, L. Xiao, F. Luo, *Inorg. Chem.,* 2020, **59**, 4995-5003.

20 Y. Liang, T. Xia, Z. Wu, Y. Yang, Y. Li, Z. Sui, C. Li, R. Fan, X. Tian and Q. Chen, *Today Chem.,* 2022, **24**, 100777.

21 D. Mullangi, V. Dhavale, S. Shalini, S. Nandi, S. Collins, T. Woo, S. Kurungot and R. Vaidhyanathan, *Adv. Energy Mater.,* 2016, **6**, 1600110.

22 S. Nandi, S. K. Singh, D. Mullangi, R. Illathvalappil, L. George, C. P. Vinod, S. Kurungot and R. Vaidhyanathan, *Adv. Energy Mater.,* 2016, **6**, 1601189.

23 Z. Gan, S. Lu, L. Qiu, H. Zhu, H. Gu and M. Du, *Chem. Eng. J.,* 2021, **415**, 127850.

24 G. Cai, L. Zeng, L. He, S. Sun, Y. Tong and J. Zhang, *Chem. Asian J.*, 2020, **15**, 1963-1969.

25 S. Yuan, L. Cui, X. He, W. Zhang and T.Asefa, *Int. J. Hydrogen Energ.*, 2020, **45**, 28860-28869.